



Development of a Multi-Band High-Sensitivity Polarization-Independent Absorber: A Biosensor for Simultaneous Detection of Multiple Cancer Biomarkers

Yousef Rafighirani¹ · Javad Javidan¹ · Hamid Heidarzadeh¹

Received: 30 May 2024 / Accepted: 23 July 2024

© The Author(s), under exclusive licence to Springer Science+Business Media, LLC, part of Springer Nature 2024

Abstract

Traditionally, biosensors are indeed designed to detect one specific analyte. However, recent advancements in biosensor technology have enabled the development of multiplexed biosensors capable of detecting multiple analytes simultaneously. This work proposes the detection of cervical cancer (HeLa cells), skin cancer (basal cells), and breast cancer (MDA-MB-231 cells) by analyzing the refractive index of these cells. This analysis is based on comparing the absorption spectra of healthy and cancerous cells. The proposed structure comprises three layers: a copper layer with a conductivity of 5.18×10^7 S/m, a silicon dioxide layer with a refractive index of 3.9 containing a cross-shaped hole with a depth of 3.5 μm , and a graphene layer. For the basal cell biosensor, the graphene layer is assigned a chemical potential of 0.7 eV; for the HeLa cell biosensor, it is 0.8 eV, and for the MDA-MB-231 cell biosensor, it is 0.9 eV. The absorption output extracted from CST software yields the highest sensitivity values. For basal cell detection, the highest sensitivity (7100) and a figure of merit (FOM) of 22 are achieved in mode B. For HeLa cell detection, a sensitivity of 5250 and FOM of 28 are attained in mode B. Finally, for MDA-MB-231 detection, a sensitivity of 5357 and FOM of 23 are achieved in mode B. This innovation is particularly beneficial in complex biological samples where the presence of multiple analytes may provide more comprehensive diagnostic information. The proposed multi-band high-sensitivity polarization-independent absorber serves as a notable example of this trend, demonstrating the potential for biosensors to evolve toward simultaneous detection of multianalyte targets, such as different types of cancer cells.

Keywords Bioreceptor · Biosensor · Graphene structure · Metamaterial · Reflection index · Cancer cells · Blood components

Introduction

In recent years, there has been a significant focus on research and development based on surface plasmon resonance (SPR). This technology has gained attention in various applications such as energy harvesting [1–3], thermal emitters [4–7], and biosensors [8–12]. So far, many plasmonic sensors based on different nanostructures have been reported. At the same time, due to the high research value of complete absorption in light-emitting diodes, optical filters, sensors, and energy harvesting, considerable costs have

been incurred in researching frequency absorbers that can be used in the design of biological sensor structures and optical switches [13–15]. So far, researchers have proposed absorption schemes in the visible, infrared, terahertz, and gigahertz ranges [16, 17]. Additionally, nanomaterial absorbers can generate multiple absorption peaks in different frequency bands, such as single-band [18, 19] and dual-band [20, 21]. Absorbers made of graphene cut into patterns can also create different absorption frequencies [22–24].

Graphene has been extensively studied due to its excellent mechanical, electrical, magnetic, and thermal properties [25–27]. The use of graphene-based surface plasmon resonance (SPR) is a real-time, label-free technique. In this context, there is still a need to introduce low-cost sensors that offer higher sensitivity [28]. With its unique features in terms of dynamic tunability and broad spectral response, graphene provides unique research capabilities in the field of

✉ Javad Javidan
Javidan@uma.ac.ir

¹ Department of Electrical and Computer Engineering,
University of Mohaghegh Ardabili, Ardabil, Iran

nanotechnology. It can be used in optical electronic devices, biological or chemical sensors, super-absorbent materials, and optical detectors [29–33]. In the infrared (IR) and terahertz range, graphene can utilize plasmon amplification to create strong light-matter interactions and improve the rate of optical absorption [34, 35]. Important researches have been done by researchers to increase the sensitivity and other performance parameters of the biosensors by using composite materials, such as the use of $\text{BK}_7/\text{Ag}/\text{STO}/\text{MoS}_2$ material, which has a sensitivity of $32140^\circ/\text{RIU}$ at a wavelength of 633 nm [32]. Also, a plasmonic sensor based on 2D inorganic with interlayer Ti MXene and SrTiO_3 that to e SrTiO_3 a sensitivity of $438.4^\circ/\text{RIU}$ can be obtained. By using the reflectance and intensity difference method, they have reached a very high sensitivity [33]. The infrared spectroscopy technique is a powerful analysis method that can be used to obtain information about the chemical composition of most samples [34]. Infrared spectroscopy is both label-free and non-destructive, making it practically useful for analyzing biological samples such as proteins, blood components, and cancer [35]. A biosensor is a device used to detect analyte samples with various characteristics. Since no labels are attached to molecules, real information and the nature of biodegradable materials remain untouched. Biological sensors can also be used in cancer research to analyze target cell lines or protein changes in cells [36].

The development of the multi-band high-sensitivity polarization-independent absorber marks a significant stride in biosensor innovation, particularly in the realm of cancer diagnostics. This advanced biosensing platform showcases the capability to simultaneously detect multiple cancer biomarkers, a crucial advancement considering the heterogeneity and complexity of cancer. By leveraging the refractive index differences between healthy and cancerous cells, this biosensor offers a promising approach to early cancer detection. Its design, featuring three distinct layers including copper, silicon dioxide, and graphene, enables efficient detection of various cancer types such as cervical, skin, and breast cancer. The integration of graphene with tailored chemical potentials for specific cancer cell types further enhances the sensor's sensitivity and selectivity. With its high sensitivity and multi-band capability, this biosensor not only provides valuable insights into cancer biology but also holds immense potential for improving cancer diagnosis and personalized treatment strategies.

Cancer (Blood Sample)

Hematologic cancers typically originate in the bone marrow and result in the production of a large number of abnormal white blood cells. These white blood cells (WBCs) are not fully formed and are known as blasts or leukemia cells.

Symptoms include bleeding and bruising, extreme fatigue, increased risk of infection, and fever. These symptoms are due to a deficiency of healthy blood cells. Diagnosis of this disease is done through blood tests and bone marrow biopsy. The four main types of leukemia are acute lymphoblastic leukemia (ALL), acute myeloid leukemia (AML), chronic lymphocytic leukemia (CLL), and chronic myeloid leukemia (CML), which is less common. Leukemia is part of a broader group called neoplasms, which includes blood, bone marrow, and the lymphatic system, and is known for blood and lymphoid tumors [37].

In 2012, 352,000 people worldwide were diagnosed with blood cancer, resulting in 265,000 deaths. This disease is the most common type of cancer among children, accounting for three-fourths of childhood blood cancers, all of which are ALL. However, almost 90% of leukemia cases are diagnosed in adults. AML and CLL are the most common types in adults. This disease is more prevalent in developed countries [38]. Treatment for this disease may include chemotherapy, radiation therapy, and bone marrow or stem cell transplantation. Biomarkers are molecules, genes, or cells that serve as markers for desired characteristics in a cell, tissue, or living system. These biomarkers are used to diagnose, complete treatment, and predict diseases. Once the biomarkers bind to the target cell, they can enable the process of cell detection and analysis. These biomarkers may be used as a way to more accurately diagnose diseases, such as the detection and analysis of cancer cells. Also, biomarkers can help predict treatment complications or disease remission. Using biomarkers, researchers and clinicians can identify target cells more precisely and better than possible.

Basal Cells

Basal cells are a type of cell found in the deepest layer of the epidermis, which is the outermost layer of the skin. These cells are responsible for constantly dividing and replenishing the skin's upper layers. Basal cells play a crucial role in skin regeneration and wound healing. When basal cells undergo uncontrolled growth, it can lead to the development of basal cell carcinoma, which is the most common type of skin cancer [43, 44].

HeLa Cells

HeLa cells are a type of immortalized human cell line that was derived from cervical cancer cells taken from Henrietta Lacks in 1951. These cells are widely used in scientific research due to their ability to divide indefinitely in culture, making them valuable for studying cell biology, genetics, and disease mechanisms. The name “HeLa” is derived from the first two letters of Henrietta Lacks' first and last names [45, 46].

MDA-MB-231 Cells

MDA-MB-231 cells are a commonly used human breast cancer cell line in research. These cells are triple-negative breast cancer cells, meaning they do not express the estrogen receptor (ER), progesterone receptor (PR), or human epidermal growth factor receptor 2 (HER2). MDA-MB-231 cells are known for their aggressive and invasive characteristics, making them a valuable model for studying breast cancer metastasis and drug resistance.

Researchers often use MDA-MB-231 cells to investigate various aspects of breast cancer biology, including tumor growth, migration, invasion, and response to different treatments. Studying these cells can provide insights into the underlying mechanisms of breast cancer progression and identify potential therapeutic targets for the development of novel anti-cancer therapies [47–49].

Materials and Methods

In this study, SPR sensors are investigated to detect multiple cancer biomarkers. A small change in the refractive index of the surrounding plasmonic medium due to biomarkers results in a shift in the peak wavelength of their spectrum. For absorption spectrum calculations, the parameters *S* and FOM in the biosensor are calculated using Eqs. 1 and 2, respectively. For further comparison, the values of refractive index change (Δn), peak wavelength shift ($\Delta\lambda$), sensitivity (*s*), and figure of merit (FOM) for the proposed structures at each cancer are calculated in a table [46].

$$S = \frac{\Delta\lambda}{\Delta n} \tag{1}$$

$$FOM = \frac{S}{FWHM} \tag{2}$$

The structure of the absorber for designing a biosensor containing a layer of graphene was designed and simulated using CST software. The simulated structure consists of three layers: the initial layer is made of copper with an electrical conductivity of 5.183×10^7 s/m [47] and cubic dimensions of $2 \mu\text{m} \times 2 \mu\text{m} \times 0.5 \mu\text{m}$, the middle layer is made of silicon dioxide with a dielectric constant of 3.9 [52, 53] and cubic dimensions of $2 \mu\text{m} \times 2 \mu\text{m} \times 5 \mu\text{m}$. The method of fabricating the proposed structure is that a layer of silicon dioxide is placed on the copper layer with the dimensions specified in the figure and using the standard lithography process and chemical vapor deposition (CVD) which is a vacuum deposition method. We create

the desired shape on silicon dioxide and then a graphene layer grown on a thin layer of silicon dioxide with a thickness of $0.1 \mu\text{m}$ is placed on the silicon dioxide layer as a cover. A graphene layer is placed on this structure, considering the graphene relaxation time $\tau = 3.6$ ps and chemical potential $\mu = 0.9$ eV at a temperature of 300 K.

In this article, three cancer samples are discussed for diagnosis. The first sensor is for basal cell detection with a chemical potential of 0.7 eV for graphene, the second sensor is to detect HeLa cell with a chemical potential of 0.8 eV for graphene, and the third sensor is intended for the detection of MDA-MB-231 cell with a chemical potential of 0.9 eV for graphene biosensor. The blood sample containing basal cell, HeLa cell, and MDA-MB-231 cell is directed into a guiding channel, at the bottom of which there are biosensors with receptors for basal cell, HeLa cell, and MDA-MB-231 cell. When the samples to be assessed are placed on their respective receptors, they cause a change in the refractive index of the reflected waves, which is detected by the amount of this refractive index change, revealing the nature of the sample as either healthy or cancerous.

As shown in Fig. 1, the general structure of the biosensor consists of a guiding channel for the passage of the samples to be assessed, the biosensor part which contains a large number of absorber structures arranged periodically next to each other, and the cellular receptors installed on the absorber structure to separate and assess the desired cell from other cells. In this structure, a large number of samples can be assessed, and in this article, three samples, basal cell, HeLa cell, and MDA-MB-231 cell, have been assessed.

The prism can be mounted on a rail system, facilitating precise and controlled adjustments to its position. This setup allows for highly accurate alignment and measurement processes. By integrating a microprocessor, the entire

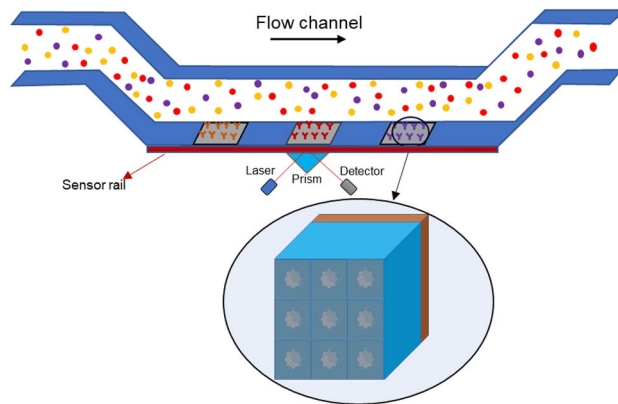


Fig. 1 The overall structure of the designed biosensor for simultaneous detection of multiple cancer biomarkers, the prism, laser, and detector are placed on a rail

measurement sequence can be automated, ensuring consistent and reliable data collection. This automation capability also enables rapid switching between different structures and materials, significantly increasing the efficiency of the measurement process. In this method, only one prism and laser structure are needed, which simplifies the experimental setup and reduces costs. The rail system allows for easy repositioning of the prism, while the microprocessor handles the adjustments and measurements. This combination enables the system to seamlessly transition between various materials without the need for multiple prisms or complex manual adjustments. The flexibility offered by this system is particularly advantageous in research and development settings, where multiple materials and configurations need to be tested quickly and accurately.

Simulation Results and Discussion

To initiate the simulation process, we first establish the material parameters and structural characteristics of our proposed multi-band high-sensitivity polarization-independent absorber. This involves defining the geometrical layout, material properties, and operating principles of the biosensor. By meticulously configuring these initial conditions, we aim to accurately model the interaction between incident electromagnetic waves and the absorber structure across multiple frequency bands. Through rigorous simulation, we anticipate gaining insights into the absorber's performance in detecting and distinguishing various cancer biomarkers simultaneously.

Figure 2 illustrates the absorption spectra of the structure of the octagonal absorber, and based on the extracted output

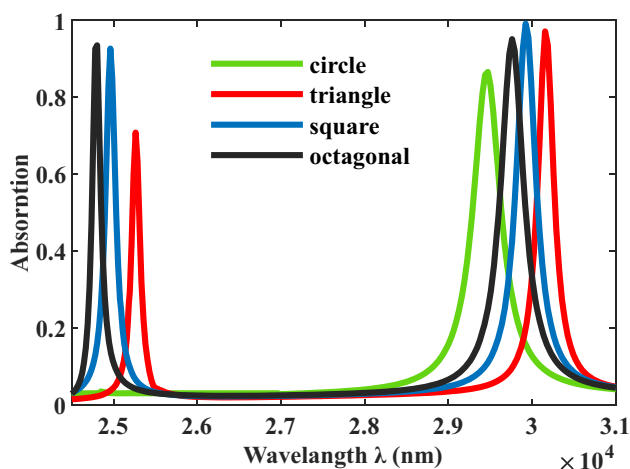


Fig. 2 Absorption waveform of the structure in the cavity states created in the form of a cylinder with a cross-section of a circle, triangle, square, and octagon

from its absorption, we conclude that the regular octagonal structure formed at the intersection of two squares with a diameter of one micron creates two waves with the highest absorption value, as well as two regular and proportional waves. Therefore, we choose this structure for designing biosensors.

In the next step, the depth of the hole is varied to select the highest absorption value. Depths of 1.5 μm , 2.5 μm , 3.5 μm , and 4.5 μm are considered, and based on Fig. 3, which shows the absorption wave output, a depth of 3.5 μm provides a more suitable absorption value. Therefore, we choose a depth of 3.5 μm in the created structure.

Figure 4a shows the structure and Fig. 4b shows the absorption spectra for different chemical potentials. Based on Table 1 and Fig. 4b, the structure in two modes with different wavelengths exhibits high absorption levels, and the absorption waveform has minimal overlap and a high-quality factor. By adjusting the chemical potential of graphene from 0.7 to 0.8 eV and 0.9 eV, the absorption wavelength changes, highlighting one of graphene's key advantages. Given the advantages of the proposed structure, it can be utilized as a biosensor. With the ability to alter the absorption wavelength by adjusting the chemical potential, a variety of biosensor structures with different chemical potentials and absorption wavelengths can be created, enabling the detection of numerous substances.

Figure 5 presents a visual representation of the absorption spectra obtained at various wavelengths through analysis conducted within the CST program. This visualization serves to elucidate the nuanced relationship between absorption wavelength and the refractive index alterations within the analyte sample. Further insights into this correlation are expounded upon in Table 2, where precise values extracted from Fig. 5 are delineated for comprehensive understanding. Moreover,

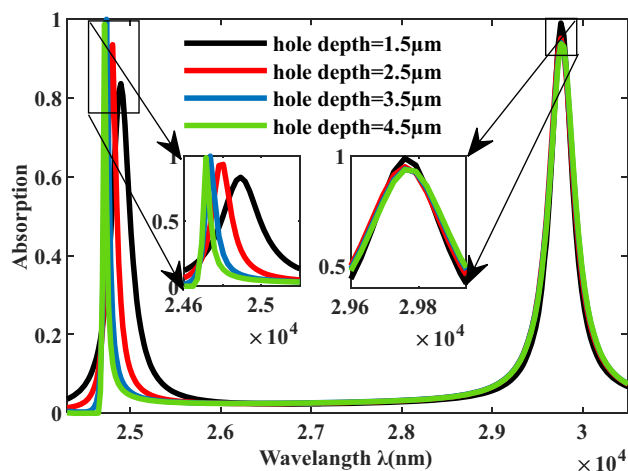
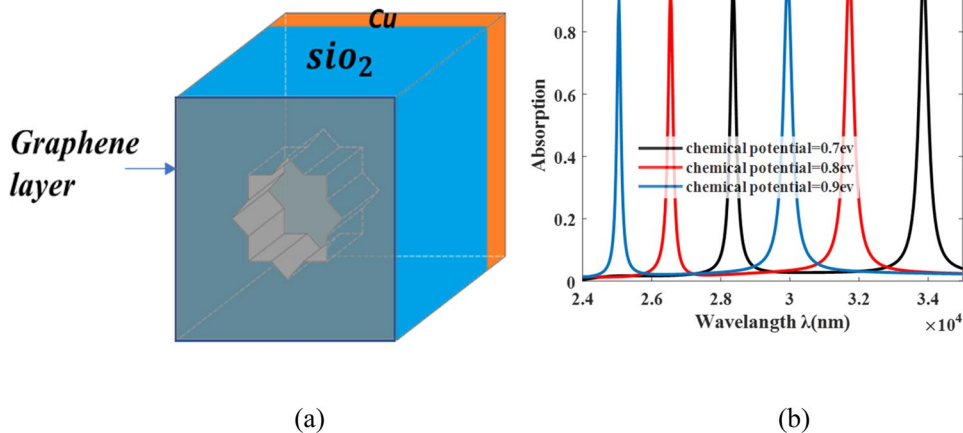


Fig. 3 Absorption waveform for the hole depth created in silicon dioxide with sizes of 1.5 μm , 2.5 μm , 3.5 μm , and 4.5 μm

Fig. 4 **a** Adsorbent structure proposed for use as biosensor. **b** Absorption waveform at chemical potential of 0.7 eV, 0.8 eV, and 0.9 eV applied to graphene



beyond mere data depiction, Fig. 5 also serves as a conduit for evaluating the biosensor’s performance. Parameters such as sensitivity and figure of merit (FOM) are meticulously calculated and furnished alongside the spectral data. These metrics are pivotal in gauging the efficacy and reliability of the biosensor, providing invaluable insights into its practical utility and potential for real-world applications.

By comparing the results of sensitivity and FOM of previously reported references, it is clear that there is a trade-off between these two parameters. In reference [50], the sensitivity has been reported as 11,500, but the FOM is relatively low at 3.9. This indicates a high sensitivity but a less efficient overall performance. In reference [51], the sensitivity drops significantly to 1700, but the FOM increases to 10.8. This threefold increase in FOM suggests a better-balanced performance despite the lower sensitivity. Reference [52] shows a continued increase in FOM compared to the previous references, indicating improved efficiency. However, the sensitivity continues to decrease relative to the earlier references. Reference [53] presents a structure very similar to the one proposed in this article. Here, the sensitivity drops drastically to 598.9, but the FOM reaches its highest value at 85.68. This implies an exceptionally high efficiency, albeit with a substantial reduction in sensitivity. When comparing these references,

it becomes evident that the proposed structure in this article strikes a favorable balance between sensitivity and FOM. With a sensitivity of 7100 and a FOM of 22, the proposed structure offers both a high sensitivity and a significantly improved FOM. This makes it a more acceptable and advantageous solution compared to the other referenced structures. The proposed structure achieves a notable improvement in overall performance by maintaining a relatively high sensitivity while also enhancing the efficiency as indicated by the FOM (Table 3).

Independent of Polarization

The advent of the multi-band high-sensitivity absorber represents a breakthrough in biosensing technology, offering a novel avenue for the simultaneous detection of multiple cancer biomarkers with unprecedented precision. This cutting-edge biosensor operates independently of polarization, enhancing its versatility and applicability across diverse biological samples. Cancerous cells typically exhibit different refractive indices compared to their healthy counterparts due to variations in their internal structure and composition. These differences can be attributed to changes in cell density, organelle size, and the overall arrangement of cellular components. By accurately measuring these variations, it is possible to detect the presence of cancerous cells at an early stage, potentially improving the prognosis and treatment outcomes. Based on the output in Fig. 6, it can be observed that the resonance peak value does not change with a change in polar angle from 0° to 120° and 270°. The shape of the graph remains constant at three polar angles, indicating the independence of the structure from changes in the polar angle. This feature of independence from the polar angle of the proposed structure makes the biosensor more practical and usable in detecting the desired analyte.

Table 1 Absorption values, wavelength peak, and waveform quality factor are included in chemical potential 0.7 eV, 0.8 eV, and 0.9 eV

Chemical potential (eV)	Mode	Absorb	λ_{pick} (nm)	Q
$\mu = 0.7$	Mode A	0.955	28365	246
	Mode B	0.995	33863	102
$\mu = 0.8$	Mode A	0.938	26542	153
	Mode B	0.987	31734	108
$\mu = 0.9$	Mode A	0.90	25053	170
	Mode B	0.968	29922	75

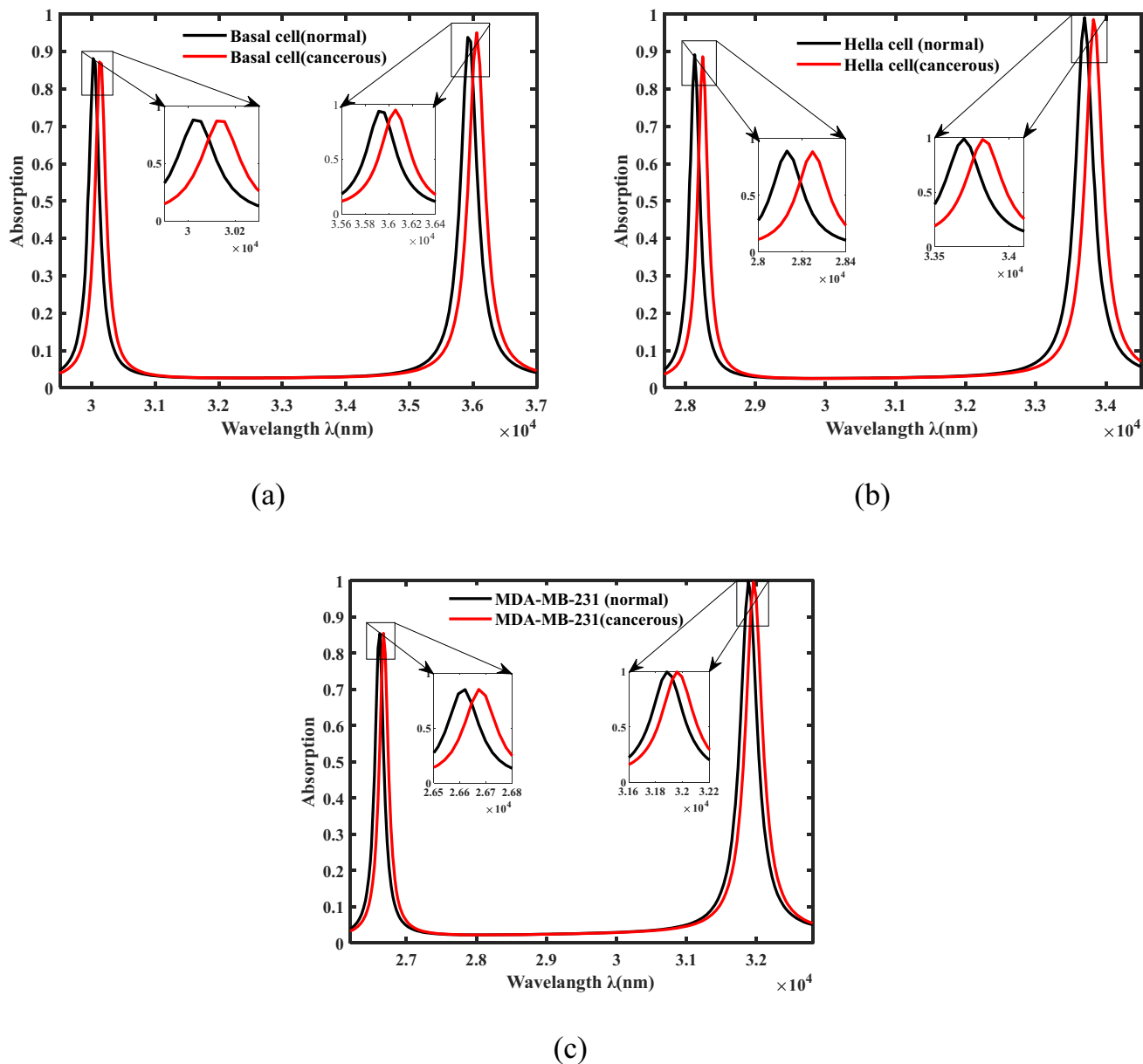


Fig. 5 Absorption waveform extracted from the biosensor from three samples. **a** Basal cell. **b** HeLa cell. **c** MDA-MB-231

Table 2 Total diagnostic parameters proposed by the biosensor for three types of cancer

Analytic used	RI	λ (nm)	Absorption (%)	FWHM	FOM	Sensitivity (nm/RIU)
Basal cell (normal)	1.360	30,021	87.2	208	–	Ref
		35,916	93.8	319	–	Ref
Basal cell (cancerous)	1.380	30,120	88	210	23	4950
		36,058	95	321	22	7100
HeLa cell (normal)	1.368	28,131	89	171	–	Ref
		33,695	99	303	–	Ref
HeLa cell (cancerous)	1.392	28,247	88.5	170	28	4833
		33,821	98.5	298	17.6	5250
MDA-MB-231 (normal)	1.385	26,619	85.3	155	–	Ref
		31,882	99.8	298	-	Ref
MDA-MB-231 (cancerous)	1.399	26,671	85.4	156	23	3714
		31,957	99.8	293	18	5357

Table 3 Comparison of the output of the proposed structure with previous works

Ref	[53]	[52]	[51]	[50]	Present
Sensitivity (nm/RIU)	598.9	1445	1700	11,500	7100
FOM	85.68	28.8	10.8	3.9	22

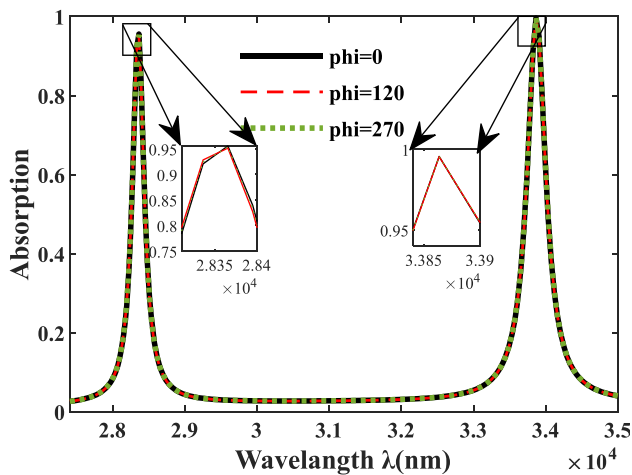


Fig. 6 Absorption waveform at the resonance peak by changing the polarization angle from 0, 120, and 270°

Conclusion

The development of a multi-band high-sensitivity polarization-independent absorber represents a significant leap forward in biosensor technology, particularly in the realm of simultaneous

detection of multiple cancer biomarkers. This advancement holds immense promise in early cancer diagnosis, a crucial factor in improving patient outcomes and reducing mortality rates. By harnessing the absorber’s capability to operate across multiple frequency bands with high sensitivity and independence from incident polarization, we can enhance the accuracy and efficiency of cancer detection. This breakthrough is particularly timely given the increasing prevalence of cancer and the urgent need for more effective diagnostic tools. Moving forward, integrating this innovative biosensor into clinical practice could revolutionize cancer screening processes and pave the way for more personalized and targeted treatment approaches. The designed biosensor boasts superior sensitivity compared to existing counterparts.

Author Contribution All authors contributed to the study conception, design, Material preparation, data collection and analysis. We confirm that the manuscript has been read and approved by all named authors and that there are no other persons who satisfied the criteria for authorship but are not listed. We further confirm that the order of authors listed in the manuscript has been approved by all of us. We understand that the Corresponding Author is the sole contact for the Editorial process. He/she is responsible for communicating with the other authors about progress, submissions of revisions and final approval of proofs Signed by all authors as follows: Yousef Rafighirani Javad Javidan Hamid Heidarzadeh.

Funding The authors did not receive support from any organization for the submitted work.

Data Availability No datasets were generated or analysed during the current study.

Declarations

Competing Interests The authors declare no competing interests.

References

- Qin F et al (2020) Ultra-broadband and wide-angle perfect solar absorber based on TiN nanodisk and Ti thin film structure. *Sol Energy Mater Sol Cells* 211:110535
- Yu P et al (2020) Ultra-wideband solar absorber based on refractory titanium metal. *Renew Energy* 158:227–235
- Zhao F et al (2020) Study on the solar energy absorption of hybrid solar cells with trapezoid-pyramidal structure based PEDOT: PSS/c-Ge. *Sol Energy* 204:635–643
- Wu P, Zhang C, Tang Y, Liu B, Lv L (2020) A perfect absorber based on similar Fabry-perot four-band in the visible range. *Nanomaterials* 10(3):488
- Zhang Y et al (2020) Study on temperature adjustable terahertz metamaterial absorber based on vanadium dioxide. *Ieee Access* 8:85154–85161
- Li J et al (2020) Tunable broadband solar energy absorber based on monolayer transition metal dichalcogenides materials using Au nanocubes. *Nanomaterials* 10(2):257
- Pan M et al (2020) A narrowband perfect absorber with high Q-factor and its application in sensing in the visible region. *Results Phys* 19:103415
- Wang X et al (2019) A theoretical study of a plasmonic sensor comprising a gold nano-disk array on gold film with a SiO₂ spacer. *Chin Phys B* 28(4):044201
- Wang X et al (2020) Surface plasmons and SERS application of Au nanodisk array and Au thin film composite structure. *Opt Quantum Electron* 52(5):238. <https://doi.org/10.1007/s11082-020-02360-2>
- Wu Y et al (2020) Surface-enhanced Raman scattering based on hybrid surface plasmon excited by Au nanodisk and Au film coupling structure. *Phys Lett A* 384(23):126544
- Chen J et al (2018) Enhancing the magnetic plasmon resonance of three-dimensional optical metamaterials via strong coupling for high-sensitivity sensing. *J Light Technol* 36(16):3481–3485
- Li L, Yang W-X, Shui T, Wang X (2020) Ultrasensitive sizing sensor for a single nanoparticle in a hybrid nonlinear microcavity. *IEEE Photonics J* 12(3):1–8
- Qi Y, Liu C, Hu B, Deng X, Wang X (2021) Tunable plasmonic absorber in THz-band range based on graphene arrow-shaped metamaterial. *Res Phys* 23:104044
- Di L, Yang H, Xian T, Chen X (2018) Facile synthesis and enhanced visible-light photocatalytic activity of novel p-Ag₃PO₄/n-BiFeO₃ heterojunction composites for dye degradation. *Nanoscale Res Lett* 13(1):257. <https://doi.org/10.1186/s11671-018-2671-6>
- Di L, Yang H, Xian T, Liu X, Chen X (2019) Photocatalytic and photo-Fenton catalytic degradation activities of Z-scheme Ag₂S/BiFeO₃ heterojunction composites under visible-light irradiation. *Nanomaterials* 9(3):399
- He Z et al (2020) Tunable Fano resonance and enhanced sensing in a simple Au/TiO₂ hybrid metasurface. *Nanomaterials* 10(4):687
- Qi Y et al (2019) Theoretical study of a multichannel plasmonic waveguide notch filter with double-sided nanodisk and two slot cavities. *Results Phys* 14:102506
- Li W, Cheng Y (2020) Dual-band tunable terahertz perfect metamaterial absorber based on strontium titanate (STO) resonator structure. *Opt Commun* 462:125265
- Cheng Y, Fan J, Luo H, Chen F (2019) Dual-band and high-efficiency circular polarization convertor based on anisotropic metamaterial. *IEEE Access* 8:7615–7621
- Cheng Y et al (2019) Dual-band and high-efficiency circular polarization conversion via asymmetric transmission with anisotropic metamaterial in the terahertz region. *Opt Mater Express* 9(3):1365–1376
- Wang Y, Jiang F, Chen J, Sun X, Xian T, Yang H (2020) In situ construction of CNT/CuS hybrids and their application in photodegradation for removing organic dyes. *Nanomaterials* 10(1):178
- Norouzi-Razani A, Rezaei P (2022) Multiband polarization insensitive and tunable terahertz metamaterial perfect absorber based on the heterogeneous structure of graphene. *Opt Quantum Electron* 54(7):407. <https://doi.org/10.1007/s11082-022-03813-6>
- Razani AN, Rezaei P (2021) Multiband polarization insensitive and tunable terahertz metamaterial perfect absorber based on the heterogeneous structure of graphene. [Online]. Available: <https://www.researchsquare.com/article/rs-438846/latest>. Accessed 12 Feb 2024
- Zamzam P, Rezaei P, Khatami SA (2021) Quad-band polarization-insensitive metamaterial perfect absorber based on bilayer graphene metasurface. *Phys E Low-Dimens Syst Nanostructures* 128:114621
- Wang J et al (2020) High-performance 2.6 V aqueous symmetric supercapacitor based on porous boron-doped diamond via regrowth of diamond nanoparticles. *Carbon* 160:71–79
- Qi Y et al (2020) A tunable terahertz metamaterial absorber composed of hourglass-shaped graphene arrays. *Nanomaterials* 10(3):533
- Liu X et al (2018) Quantitatively optical and electrical-adjusting high-performance switch by graphene plasmonic perfect absorbers. *Carbon* 140:362–367
- Saadatmand SB, Chemerkouh MJHN, Ahmadi V, Hamidi SM (2023) Graphene-based integrated plasmonic sensor with application in biomolecule detection. *JOSA B* 40(1):1–10
- Rafighirani Y, Javidan J, Heidarzadeh H (2024) Polarization-independent tunable multi-band terahertz absorber based on graphene structure to design the ultra-high sensitive biosensors. *Phys Scr* 99(7):075014
- Qi Y, Zhang B, Liu C, Deng X (2020) Ultra-broadband polarization conversion meta-surface and its application in polarization converter and RCS reduction. *Ieee Access* 8:116675–116684
- Wang S et al (2020) Structure characterization, optical and photoluminescence properties of scheelite-type CaWO₄ nanophosphors: Effects of calcination temperature and carbon skeleton. *Opt Mater* 99:109562
- Saadatmand SB, Chemerkouh MJHN, Ahmadi V, Hamidi SM (2023) Design and analysis of highly sensitive plasmonic sensor based on 2-D inorganic Ti-MXene and SrTiO₃ interlayer. *IEEE Sens J* 23(12):12727–12735
- Chemerkouh MJHN, Saadatmand SB, Hamidi SM (2022) Ultra-high-sensitive biosensor based on SrTiO₃ and two-dimensional materials: Ellipsometric concepts. *Opt Mater Express* 12(7):2609–2622
- Luxmoore JJ, Liu PQ, Li P, Faist J, Nash GR (2016) Graphene-Metamaterial photodetectors for integrated infrared sensing. *ACS Photonics* 3(6):936–941. <https://doi.org/10.1021/acsp Photonics.6b00226>
- Farmani A (2019) Three-dimensional FDTD analysis of a nanostructured plasmonic sensor in the near-infrared range. *JOSA B* 36(2):401–407
- Erim N, Erim MN, Kurt H (2019) An optical sensor design using surface modes of low-symmetric photonic crystals. *IEEE Sens J* 19(14):5566–5571
- Vollmer F, Arnold S (2008) Whispering-gallery-mode biosensing: label-free detection down to single molecules. *Nat Methods* 5(7):591–596
- Zhang J, Hodge W, Hutnick C, Wang X (2011) Noninvasive diagnostic devices for diabetes through measuring tear glucose. *J Diabetes Sci Technol* 5(1):166–172. <https://doi.org/10.1177/193229681100500123>

39. Fania L et al (2020) Basal cell carcinoma: from pathophysiology to novel therapeutic approaches. *Biomedicines* 8(11):449
40. Lanoue J, Goldenberg G (2016) Basal cell carcinoma: a comprehensive review of existing and emerging nonsurgical therapies. *J Clin Aesthetic Dermatol* 9(5):26
41. Masters JR (2002) HeLa cells 50 years on: the good, the bad and the ugly. *Nat Rev Cancer* 2(4):315–319
42. Zhao Y et al (2014) Three-dimensional printing of HeLa cells for cervical tumor model in vitro. *Biofabrication* 6(3):035001
43. Liu F et al (2021) Key factor regulating inflammatory microenvironment, metastasis, and resistance in breast cancer: Interleukin-1 Signaling. *Mediators Inflamm* 2021:1–18
44. Azam M (2020) The efficacy and mechanism of action of HDAC inhibitors in triple negative breast cancer. PhD Thesis, University of Otago [Online]. Available: <https://ourarchive.otago.ac.nz/handle/10523/10129>. Accessed 27 Feb 2024
45. Hamilton N et al (2015) Biologic roles of estrogen receptor- β and insulin-like growth factor-2 in triple-negative breast cancer *BioMed Res Int* 2015.[Online]. Available: <https://www.hindawi.com/journals/bmri/2015/925703/abs/>. Accessed 27 Feb 2024
46. Heidarzadeh H (2020) Analysis and simulation of a plasmonic biosensor for hemoglobin concentration detection using noble metal nano-particles resonances. *Opt Commun* 459:124940
47. Tahseen MM, Kishk AA (2016) Wideband textile-based conformal antennas for WLAN band using conductive thread in 2016 10th European Conference on Antennas and Propagation (EuCAP), IEEE, pp. 1–5. [Online]. Available: <https://ieeexplore.ieee.org/abstract/document/7481527/>. Accessed 27 Feb 2024
48. Chen P-Y, Alù A (2011) Atomically thin surface cloak using graphene monolayers. *ACS Nano* 5(7):5855–5863. <https://doi.org/10.1021/nn201622e>
49. Deng XH, Liu JT, Yuan J, Wang TB, Liu NH (2014) Tunable THz absorption in graphene-based heterostructures. *Opt Exp* 22(24):30177–30183
50. Huang J et al (2019) High sensitivity refractive index sensing with good angle and polarization tolerance using elliptical nanodisk graphene metamaterials. *Phys Scr* 94(8):085805
51. Yi Z et al (2019) Dual-band plasmonic perfect absorber based on graphene metamaterials for refractive index sensing application. *Micromachines* 10(7):443
52. Cheng Y, Mao XS, Wu C, Wu L, Gong R (2016) Infrared non-planar plasmonic perfect absorber for enhanced sensitive refractive index sensing. *Opt Mater* 53:195–200
53. Jiang L et al (2021) Multi-band and high-sensitivity perfect absorber based on monolayer graphene metamaterial. *Diam Relat Mater* 111:108227

Publisher's Note Springer Nature remains neutral with regard to jurisdictional claims in published maps and institutional affiliations.

Springer Nature or its licensor (e.g. a society or other partner) holds exclusive rights to this article under a publishing agreement with the author(s) or other rightsholder(s); author self-archiving of the accepted manuscript version of this article is solely governed by the terms of such publishing agreement and applicable law.